Coastal Upwelling: Onshore–Offshore Circulation, Equatorward Coastal Jet and Poleward Undercurrent over a Continental Shelf-Slope

NOBUO SUGINOHARA

Geophysical Institute, Faculty of Science, University of Tokyo, Bunkyo-ku, Tokyo 113, Japan

(Manuscript received 2 October 1981, in final form 9 December 1981)

ABSTRACT

The onshore–offshore circulation, equatorward coastal jet and poleward undercurrent associated with coastal upwelling are studied with numerical models. The model ocean has a continental shelf–slope uniform in the longshore direction and is forced by the wind stress with a limited longshore extent. The thermocline intersects the shelf–slope and the internal radius of deformation is smaller than the width of the shelf–slope. This may be a typical situation for coastal upwelling regions such as those off Oregon and northwest Africa. As the initial response to the onset of the winds, the Ekman offshore flow and the compensating onshore flow are induced and the equatorward flow develops over the shelf–slope. When the first mode coastal-trapped wave from the equatorward edge of the forcing region arrives, the onshore compensating flow offshore of the coastal area begins to decrease in strength and eventually offshore flow accompanied by downwelling dominates. Thus, the upwelling tends to be confined to the coastal area. For the alongshore flow, the equatorward flow tends to be confined to the coastal area, and the poleward undercurrent develops below the thermocline over the slope. When the second mode wave arrives, the upwelling is further confined to the coastal area and the equatorward coastal jet and poleward undercurrent cease to develop. Thus, coastal trapped waves, which are neither internal Kelvin nor barotropic shelf waves, play essential roles in determining the upwelling circulation.

1. Introduction

Recent observational activities off Oregon and northwest Africa have increased our knowledge of coastal upwelling (e.g., Huyer *et al.*, 1975 for off Oregon and Barton *et al.*, 1977 for off northwest Africa). Significant contributions were made by direct current measurements. The offshore and alongshore components of flow associated with the upwelling were measured. Existence of the offshore flow in the deeper part of the thermocline over the slope during upwelling events is now evident as a typical onshore–offshore circulation associated with coastal upwelling (see, e.g., Huyer, 1976). Evolution of the equatorward coastal jet and the poleward undercurrent is becoming clear.

Theoretical studies on coastal upwelling have been made by various authors (see Allen, 1980). Among them, Suginohara (1974), using a two-layer model in which the interface is shallower than shelf depth and so intersects the vertical coastal wall, demonstrated the importance of internal Kelvin and shelf waves on the coastal upwelling dynamics. He showed that the coastal upwelling is a phenomenon associated with the generation and propagation of internal Kelvin waves, and that of the shelf waves control the occurrence of the poleward undercurrent over the shelf. Recently, Yoon and Philander (1982) clarified the formation mechanism of the poleward undercurrent for a continuously stratified ocean with a flat bottom. In their model, Kelvin waves of many vertical modes play roles in the formation of the undercurrent. However, in real oceans there is a continental shelf–slope. A two-layer model (Suginohara, 1974) in which the interface intersects the vertical coastal wall may not be appropriate for representing the observed density stratification.

Wang and Mooers (1976) and Huthnance (1978) studied the coastal-trapped waves in a continuously stratified ocean in which the thermocline intersects a continental slope. They found that the identification of modes as internal Kelvin or barotropic shelf waves is not always clear, i.e., in general the possible waves involve both the topographic and stratified elements of the situation. In particular, Huthnance pointed out that the wave characteristics depend on the ratio of the radius of deformation (Lr) to the width of the slope (Ls). Waves associated with considerable thermocline displacements (internal Kelvin-type waves) exist when $Lr/Ls > 1$, but do not exist when $Lr/Ls < 1$. Suginohara (1981) demonstrated important differences in wave properties caused by the variation of the Coriolis parameter for the poleward propagation of internal Kelvin-type waves from the equatorial region. Off Oregon and northwest Africa, the ratio, Lr/Ls is definitely smaller than unity; hence, we cannot anticipate generation of internal Kelvin-type waves and cannot

0022-3670/82/030272-13$07.25

depend on the roles played by internal Kelvin-type waves in coastal upwelling dynamics.

In the present study, in order to clarify roles played by coastal-trapped waves which may be identified neither as internal Kelvin nor as barotropic shelf waves, numerical experiments are performed for a stratified ocean with a continental shelf-slope. The model ocean on an f-plane has a continental shelf-slope uniform in the longshore direction and is forced by the wind stress with a limited longshore extent. We will focus our attention on a case where the thermocline intersects the shelf-slope. This case may represent a typical situation for upwelling regions such as those off Oregon and northwest Africa.

Two case studies are discussed. For the first case, as a basic experiment, a thin thermocline, which may represent the main thermocline, is considered and characteristics of coastal-trapped waves and roles played by those waves in coastal upwelling dynamics are examined. In typical upwelling regions and during the upwelling season, the seasonal thermocline occupies the upper several tens of meters of the water column and forms a rather thick thermocline with the main thermocline. Hence, for the second case, the seasonal thermocline is included and effects of the seasonal thermocline on the upwelling circulation are studied.

In the formulation of the model equations, the rigid-lid approximation is adopted to filter out external inertio-gravitational waves such as barotropic Kelvin waves. The roles of barotropic Kelvin waves, and that of the β effect, in coastal upwelling dynamics were discussed by Yoshida (1980). The rigid-lid approximation yields a realistic description of the upwelling circulation. Under this approximation, the offshore Ekman transport is compensated two-dimensionally by the barotropic onshore flow.

Details of upwelling circulation in the shelf region such as the formation of fronts (Suginohara, 1977) will not be studied in the present paper. Special attention will be paid to gross features of coastal upwelling involving both the density stratification and the continental shelf-slope.

2. Model

We consider a stratified ocean adjacent to a meridional eastern boundary in the Northern Hemisphere. The ocean is bounded also by artificial northern, southern and western boundaries. A schematic view of the model ocean is shown in Fig. 1. The latitudinal width of the ocean is 450 km and the longitudinal width is 2700 km. The ocean has a continental shelf-slope of 130 km width, uniform in the longshore direction; and the ocean depth is 1385 m. We use a rectangular coordinate system on an f-plane with x eastward, y northward and z vertically downward from the mean sea-surface level. Let u, v and w be the components of velocity in the x, y and z directions, respectively, p pressure and ρ density. The equations of motion and the hydrostatic relation under the Boussinesq approximation are

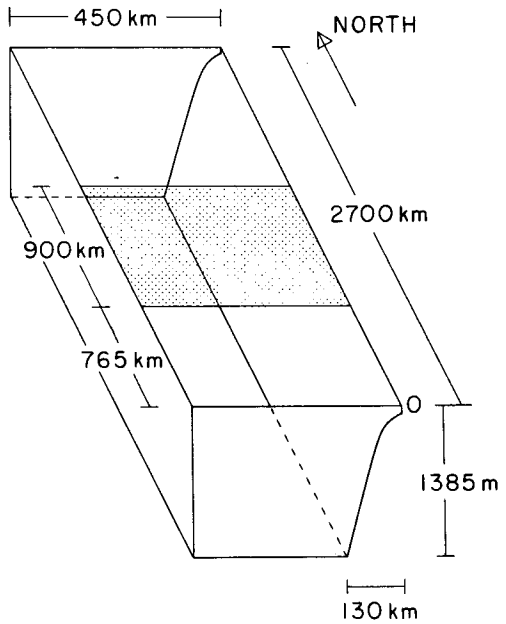

FIG. 1. Schematic view of the model ocean. The shaded zone indicates the forcing region.

$$\frac{\partial u}{\partial t}+\frac{\partial u^2}{\partial x}+\frac{\partial uv}{\partial y}+\frac{\partial uw}{\partial z}-fv = -\frac{1}{\rho_0}\frac{\partial p}{\partial x}+A_V\frac{\partial^2 u}{\partial z^2}+A_H\nabla^2 u,$$

$$\frac{\partial v}{\partial t}+\frac{\partial uv}{\partial x}+\frac{\partial v^2}{\partial y}+\frac{\partial vw}{\partial z}+fu = -\frac{1}{\rho_0}\frac{\partial p}{\partial y}+A_V\frac{\partial^2 v}{\partial z^2}+A_H\nabla^2 v,$$

$$0 = -\frac{\partial p}{\partial z}+\rho g,$$

and the equation of continuity is

$$\frac{\partial u}{\partial x}+\frac{\partial v}{\partial y}+\frac{\partial w}{\partial z}=0,$$

where A_V and A_H are the coefficients of the vertical and horizontal eddy viscosity, respectively, ρ_0 is the mean density over the whole depth, and f the Coriolis parameter, taken to be constant. The equation of density under the assumption that density and temperature have a linear relation is

$$\frac{\partial \rho}{\partial t}+\frac{\partial \rho u}{\partial x}+\frac{\partial \rho v}{\partial y}+\frac{\partial \rho w}{\partial z}=\frac{K_V}{\delta}\frac{\partial^2 \rho}{\partial z^2}+K_H\nabla^2\rho,$$

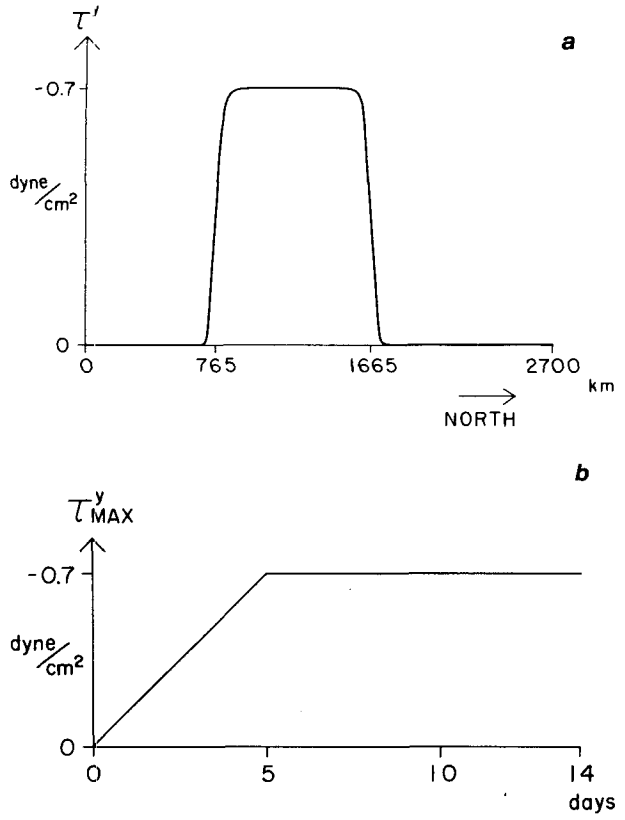

FIG. 2. (a) Longshore distribution of τ^y. (b) Time change of τ^y.

where K_V and K_H are the coefficients of the vertical and horizontal eddy diffusion, respectively. δ, a convective adjustment parameter used to maintain a stable stratification, is defined by

$$\delta = \begin{cases} 1 & \text{for } \partial\rho/\partial z > 0, \\ 0 & \text{for } \partial\rho/\partial z < 0. \end{cases}$$

In the initial state, the ocean is at rest and the stratification is horizontally uniform. The initial stratification for each of the two cases will be described in the next section.

Boundary conditions are as follows. At the coastal walls, $u = v = 0$. At the ocean bottom, $w = u\partial D/\partial x$ where D is the depth and $\partial u/\partial n = \partial v/\partial n = 0$ where n denotes the coordinate normal to the bottom. At the sea surface, $w = \partial u/\partial z = 0$ and $-A_V\partial v/\partial z = \tau^y$. The heat exchange through the boundaries is not taken into account. Only southward wind stress (τ^y) is considered. τ^y has a limited longshore extent as shown in Fig. 2a and is uniform in the x direction. For the temporal change, τ^y is assumed to increase gradually to a steady-state value within five days in order to avoid generation of inertial-internal oscillations (Fig. 2b). Setting $w = 0$ at the sea surface leads to the rigid-lid approximation; it is then possible to define a transport streamfunction

$$\int (u, v)dz = \left(-\frac{\partial\psi}{\partial y}, \frac{\partial\psi}{\partial x}\right),$$

where the integral is performed from the mean sea-surface level to the bottom. The boundary condition for the streamfunction is that the side wall is a streamline, i.e., $\psi = 0$ along the walls.

The numerical method used in the present experiment is that of Suginohara (1981). For the deepest layer, the vertical grid intervals are varied to fit the configuration of the shelf–slope, which is portrayed by a smoothed curve in Figs. 3 and 11.

The following values are used for numerical calculations; $\rho_0 = 1.0$ g cm^{-3}, $f = 4 \times 10^{-5}$ s^{-1}, $A_V = 10$ cm^2 s^{-1}, $A_H = 5 \times 10^5$ cm^2 s^{-1}, $K_V = 0.01$ cm^2 s^{-1} and $K_H = 10^3$ cm^2 s^{-1}. To avoid smoothing out the initial density stratification, the coefficients of diffusion are taken to be as small as possible. The mesh intervals are 5 km in the x direction and 30 km in the y direction. For the vertical resolution, 10 levels are taken as shown in Figs. 3 and 11.

3. Results

a. Basic experiment

The initial density stratification is shown in Fig. 3. The thin thermocline which intersects the shelf–slope is considered. The radius of deformation appropriate for the present model may be $(\Delta\rho g h)^{1/2}/f \approx 35$ km where $\Delta\rho$ (=1.2 in σ_t units) is the maximum vertical density difference and h the depth of the thermocline. The radius of deformation is smaller than the width of the shelf–slope.

Sequential patterns of the onshore–offshore circulation, alongshore flow and density deviations from the initial state along the zonal section at the center of the forcing region are shown in Figs. 4a, b and c. As the initial response to the onset of the winds, the Ekman offshore flow and the compensating onshore flow are induced and develop as the winds increase in speed. Then, the compensating onshore flow

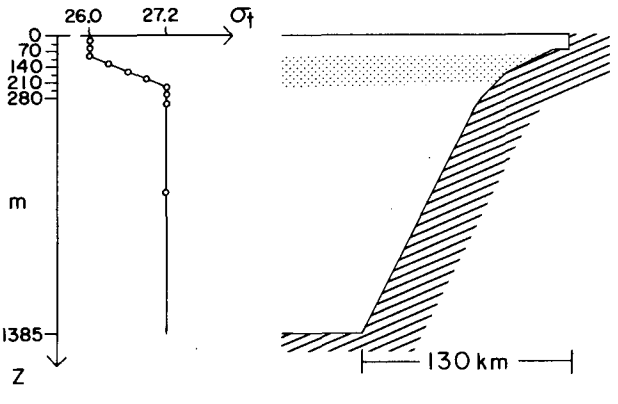

FIG. 3. The initial stratification for case A.

offshore of the coastal area decreases in strength, and offshore flow accompanied by downwelling dominates as seen at day 7. Thereafter, as found at days 10–14, the upwelling tends to be confined to the coastal area. In Fig. 4b for the alongshore flow, the equatorward flow develops over the shelf–slope as the initial response. Then, the equatorward flow tends to be confined to the coastal area, and the poleward flow tends to occupy the offshore area. At day 14, the concentrated poleward undercurrent forms below the thermocline over the slope. In Fig. 4c for the density deviations (which represent the net vertical velocity over the period), the upwelled water occupies the wide area over the slope in the early stage, and later becomes colder and is confined to a narrower area nearshore. The downwelled water tends to occupy the depths below the thermocline over the slope as seen at day 14.

To see the horizontal distributions, sequential patterns of the streamfunction, vertical velocity at the depth of 175 m, density at 157.5 m and horizontal velocity fields at 192.5 and 52.5 m are shown in Figs. 5a, b, c, d and e. Within a day or two, there is no significant longshore distribution of each variable except at the northern and southern edges of the forcing region. Thus, the upwelling circulation inside the forcing region is balanced in a two-dimensional (offshore, vertical) plane. An anticyclonic vortex in the streamfunction field is formed in the forcing region and spreads poleward with the whole forcing region being occupied by the offshore transport. For the vertical velocity and density in Figs. 5b and c (which represent motions in the lower part of the thermocline), the upwelling region spreads poleward leaving downwelling behind it. The downwelling starts at the southern edge of the forcing region, and the downwelling area spreads poleward. Figs. 5d and e clearly show motions associated with evolution of the streamfunction and density. In Fig. 5d, for velocity fields just below the thermocline, the region of the equatorward flow with an onshore component spreads poleward, with the forcing region being gradually occupied by the poleward flow with an offshore component. The offshore flow and the poleward undercurrent commence at the southern edge and tend to propagate poleward. The poleward spreading of the equatorward flow at this depth seems to correspond to that of the vortex in the streamfunction field. In Fig. 5e, showing velocity fields above the thermocline, the region of the strong equatorward flow extends poleward, which is also associated with the poleward movement of the vortex. Development of the equatorward flow ceases from the southern edge, which gives rise to the longshore gradient of the equatorward coastal jet (the detailed longshore distribution will be shown in Fig. 10e). Hence, it may be understood that in the later stages, when the upwelling is confined to the coastal area, the compensation for the upwelling (the mass budget) is maintained three-dimensionally by the divergence due to the alongshore flow as well as the onshore flow.

As found in the horizontal distributions, changes in upwelling circulation take place initially at the southern edge of the forcing region and extend poleward. To see the propagation characteristics, time evolution of the streamfunction along the line 110 km from the coast is shown in Fig. 6. This line is at the center of the vortex in Fig. 5a. In the forcing region the equatorward transport increases with time in the early stage, and ceases to develop from the southern edge, which is found in the pattern as a ridge. North of the forcing region, the ridge in the pattern is also found, but it must have different properties because there is no forcing. There, the time evolution may represent the free propagation of coastal trapped waves generated at the southern and northern edges of the forcing region. The ridge north of the forcing region may be caused by the wave from the southern edge which tends to stop development of the equatorward transport. Before and after this ridge passes through, two different propagation characteristics are found. The one found in the early stage has a propagation speed of $\sim$220 cm s^{-1}, and the other after the ridge passes through has a speed of $\sim$70 cm s^{-1}. The ridge has the same speed as the former. Thus, those two propagation characteristics may be accounted for by the free propagation of the coastal trapped waves generated at the northern edge.

Next, let us look at the motions associated with those waves. In Figs. 7a and b, the onshore–offshore circulation and alongshore flow along the zonal section 150 km north of the northern edge of the forcing region before and after the ridge passes through are depicted. At day 7 when the first signal dominates, all the zonal flows have an onshore component and the alongshore flow has minor vertical shear. But, at day 14 when the second signal dominates, significantly different onshore–offshore circulation and alongshore flow occur. There is onshore flow in the coastal area and offshore flow in the offshore area. The vertical shear of the alongshore flow increases significantly and the poleward undercurrent further develops in the deeper part of the offshore area.

Now, let us clarify the characteristics of the coastal trapped waves which exist in the present model. Fig. 8 shows a schematic view of the model originally invented by Kawabe (1982). The density stratification is represented by two layers and the interface intersects the slope. The characteristics of the shelf–slope and density stratification in the present model are well reproduced in this idealized model. The density difference between the two layers is 1.2 in σ_t units and the Coriolis parameter is 4×10^{-5} s^{-1}. The offshore and alongshore components of velocity for the lowest two modes for long non-

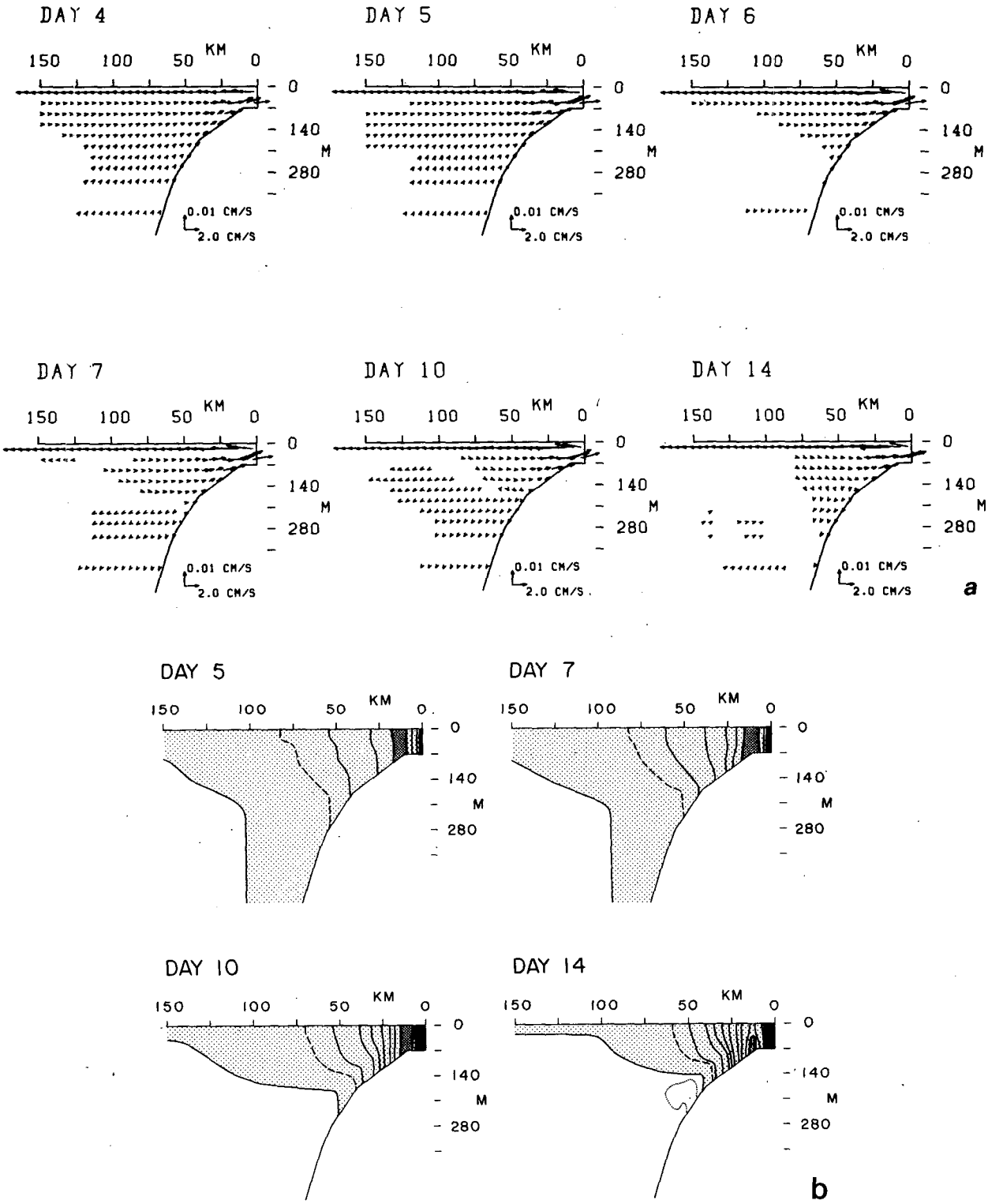

FIG. 4. Sequential patterns of the onshore–offshore circulation (a), alongshore flow (b), and deviations of density from the initial state (c), along the zonal section at the center of the forcing region. The contour intervals are 4 cm s^{-1} for the alongshore flow and 0.02 in σ_t units for density deviations. Shaded areas indicate the equatorward flow (maximum areas are hatched) and the density lighter than the initial state. For the alongshore flow, the dashed lines are for -2 cm s^{-1} and the dotted line for 1 cm s^{-1}.

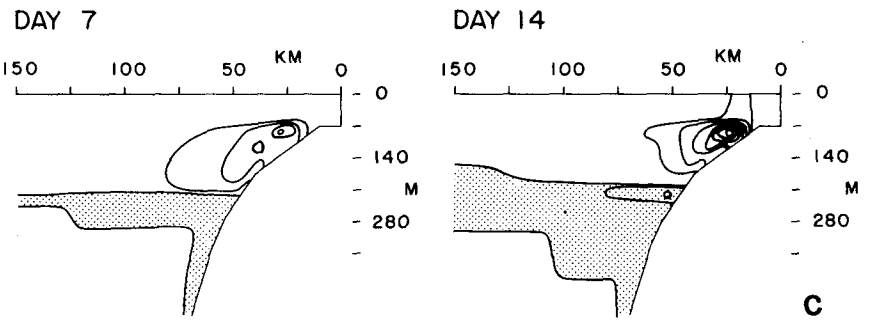

FIG. 4. (*Continued*)

dispersive waves are shown in Fig. 9. The phase speed (the group velocity) is 226 cm s^{-1} for the first mode, and 76 cm s^{-1} for the second mode. For the first mode, the motion of the upper layer is predominant over that of the lower layer, but for the second mode the lower layer motion dominates. The comparison for the onshore–offshore flow indicates that the first signal represents the first mode coastal-trapped wave, and the second signal the second mode wave, although there is a slight difference in detailed distribution of the eigenfunctions due to the thicker thermocline in the present model (compare Fig. 7a with Fig. 9). The distribution of the alongshore flow at day 7 is quite similar to the eigenfunction of the first mode in Fig. 9, and that at day 14 may be accounted for by combination of the motions accompanied by the first and second mode waves. Therefore, it may be concluded that the first and second mode coastal-trapped waves are predominantly generated at the northern edge and propagate poleward.

Next, let us account for the upwelling circulation obtained in the forcing region using propagation of the coastal-trapped waves from the southern edge. At the southern edge, the first and second mode coastal-trapped waves, whose motions are the same as those in Fig. 7 but with the opposite sense, must be predominantly generated. In Figs. 10a, b, c, d and e, y–t diagrams for the onshore–offshore flow, vertical velocity, density and alongshore flows are shown. We follow the idea proposed by Yoon and Philander (1982) for the role played by many vertical modes of Kelvin waves for a flat-bottom ocean in the formation of the poleward undercurrent. They divide the motions into the forced motions and motions associated with waves generated at the southern edge of the forcing region. The forced upwelling circulation is that found in the early stage as seen in Figs. 4a and b. The onshore–offshore circulation attains its steady state soon after the winds reach their steady-state value. The ridge in the patterns of each variable lies roughly on the line parallel to the phase line of the first mode coastal-trapped wave. Occurrence of the offshore flow (Fig. 10a), which is associated with the downwelling (Fig. 10b), is also found on the line parallel to the phase line. Those features may be understood as follows. When the first mode coastal-trapped wave (whose motions are those of Fig. 7 but with the opposite sense) arrives, the part of the forced alongshore flow corresponding to the motion associated with the first mode wave ceases to develop toward a steady state for this mode, and part of the forced onshore–offshore circulation tends to decrease in strength. The rest of the forced alongshore flow keeps developing. Eventually, the equatorward flow and upwelling are concentrated in the coastal area and the poleward undercurrent develops. It appears that the events for the onshore–offshore circulation precede those for the alongshore flow and density. This phase difference may be due to the distribution of motion associated with the wave, i.e., the change in onshore–offshore circulation occurs with the arrival of the front of the wave. We also find the other ridges in the poleward undercurrent area (Fig. 10d) and in the equatorward coastal jet (Fig. 10e). Those ridges lie roughly on the line parallel to the phase line of the second mode wave. This may be accounted for in the same way as for the first mode. When the second mode wave arrives, both the equatorward coastal jet and the poleward undercurrent cease to develop. In the forcing region, after the first mode wave passes through, the considerable longshore gradient of the equatorward coastal jet forms, which indicates the important effect of the divergence due to this jet on the mass budget.

Therefore, it may be concluded that the gross features of the upwelling circulation, such as the equatorward coastal jet, poleward undercurrent and concentration of the upwelling in the coastal area, are accounted for by coastal-trapped wave dynamics. The lowest two modes, especially the first mode, play essential roles in determining the upwelling circulation.

b. Effects of the seasonal thermocline

The initial seasonal stratification is shown in Fig. 11. The seasonal thermocline occupies the upper part

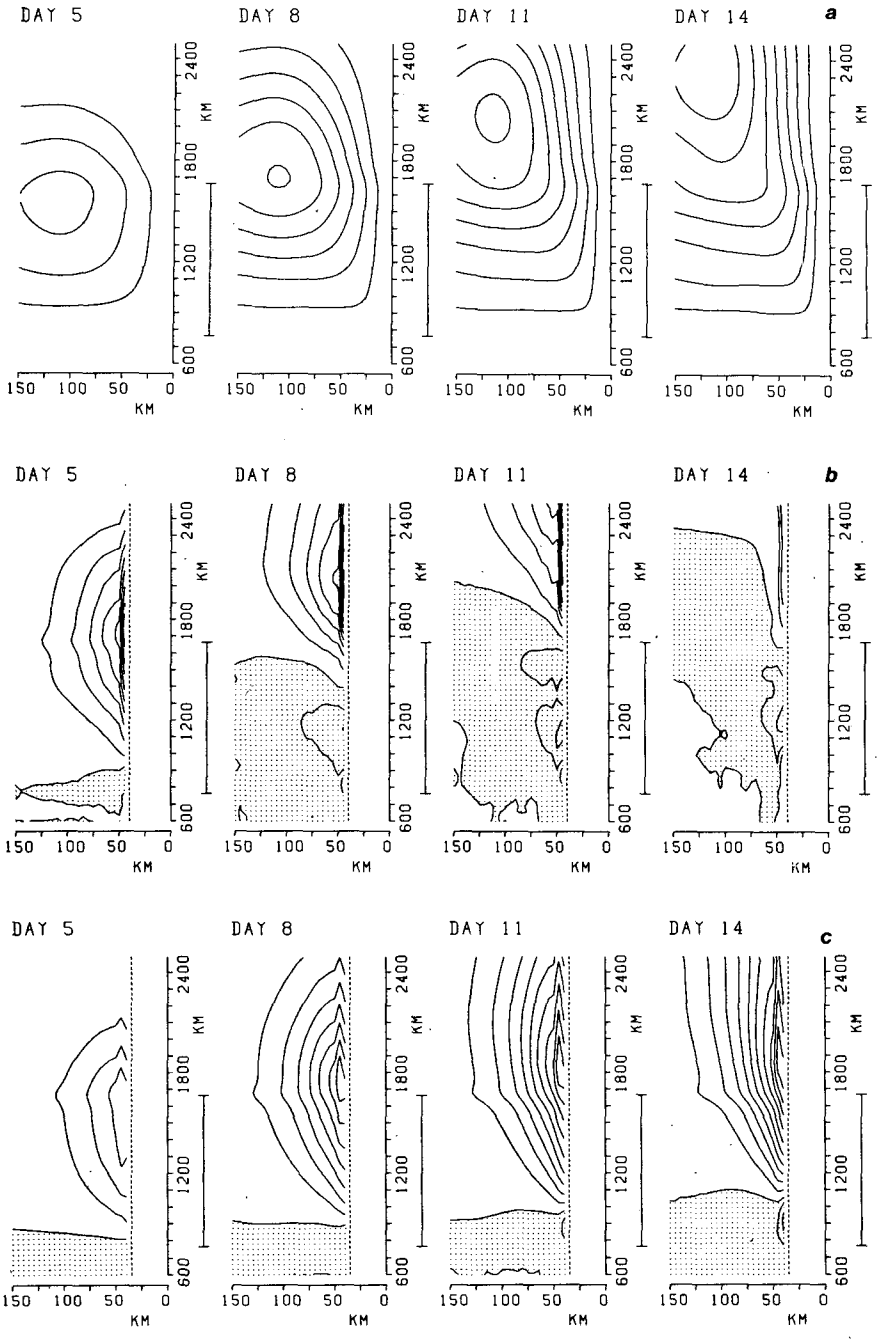

FIG. 5. Sequential patterns of the streamfunction (a), vertical velocity at the depth of 175 m (b), density at 157.5 m (c), velocity fields at 192.5 m (d), and 52.5 m (e). The contour intervals are 3×10^{11} cm^3 s^{-1} for the streamfunction, 5×10^{-4} cm s^{-1} for the vertical velocity and 0.015 in σ_t units for density. Shaded areas indicate the downwelling and the density lighter than the initial state. The forcing region is marked on the right side of each figure.

of the ocean. Figs. 12a and b show sequential patterns of the onshore–offshore circulation and alongshore flow along the section at the center of the forcing region. The patterns and evolution of the onshore–offshore circulation are similar to those of case A (compare with Fig. 4a). The offshore flow accompanied by downwelling takes place at almost the same day and the upwelling tends to be confined to the coastal area. The upwelling region at day 14 seems to be wider than in case A. For the alongshore flow, the patterns and evolution are also similar to those of case A, although the equatorward coastal jet has vertical shears (compare Fig. 12b with Fig. 4b). Fig. 13 shows the density section at day 14. As

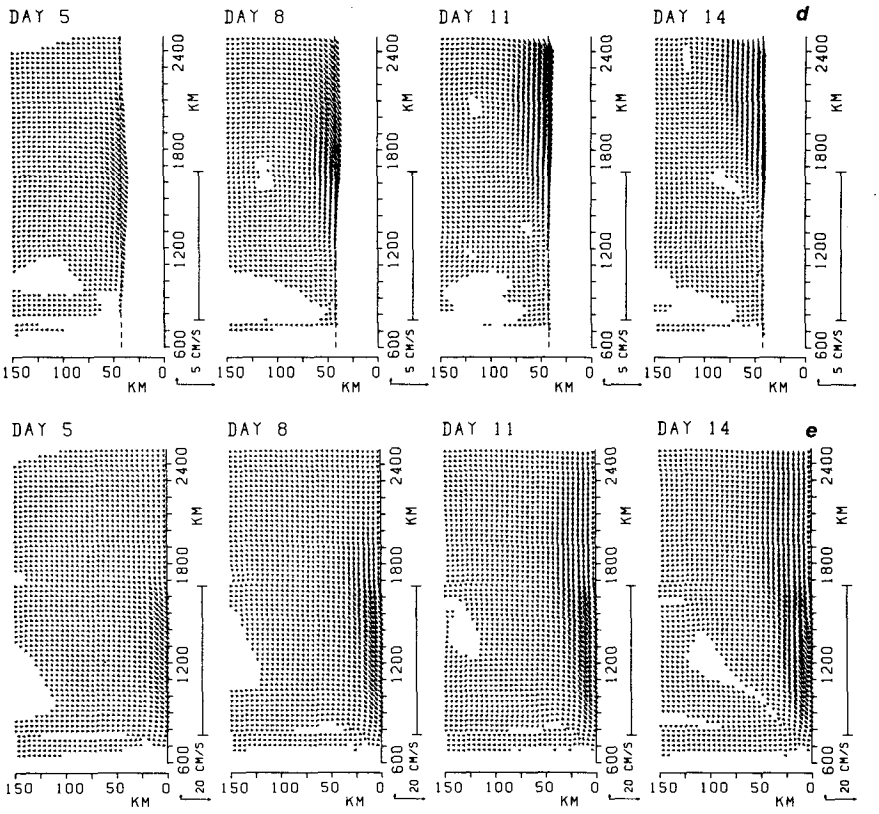

FIG. 5. (*Continued*)

the winds continue to blow the isopycnals which form the seasonal thermocline upslope toward the coast and reach the sea surface forming fronts. Circulation associated with the fronts, as studied by Suginohara (1977), is not found because of the coarse resolution in the present model.

To see the evolution of the upwelling circulation, y–t diagrams for the streamfunction, onshore–offshore flow and alongshore flow are depicted in Figs. 14a, b, c and d. It is also clearly found in this case that the concentration of the upwelling in the coastal area and the formation of the equatorward coastal jet and poleward undercurrent can be accounted for by the propagation of the coastal-trapped wave from the southern edge of the forcing region. In Figs. 15a and b, the onshore–offshore circulation and alongshore flow before and after the ridge passes through (for a position north of the forcing region in Fig. 14a) are plotted. The characteristics of the motions associated with the first and second mode waves are similar to those of case A, although motions in the upper part of the ocean are affected by the presence of the seasonal thermocline. The propagation speed of the first mode wave is very close to that in case A and that of the second is several percent smaller than in case A. Thus, the similarity in patterns and evolution of the upwelling circulation between the two cases can be understood.

Another case where the thermocline layer is thicker than in the present model was also studied. This case also shows that the characteristics of the first and second mode coastal-trapped waves are almost identical to those of cases A and B, and the patterns and evolution of the upwelling circulation are quite similar to those of cases A and B. Therefore, it is concluded that the gross features of the upwelling circulation, such as the equatorward coastal jet, poleward undercurrent and concentration of the

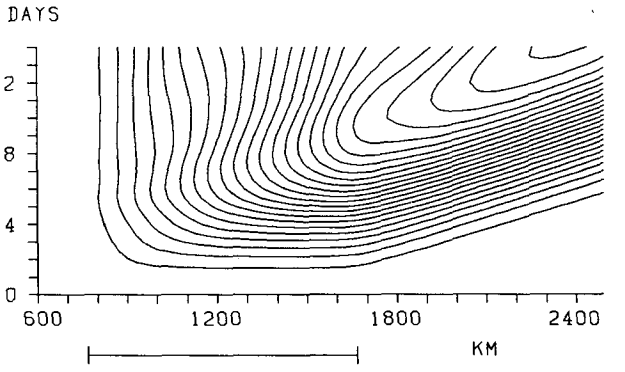

FIG. 6. y–t diagram for the streamfunction along the line 110 km from the coast. The contour interval is 10^{11} cm^3 s^{-1}. The forcing region is marked at the bottom.

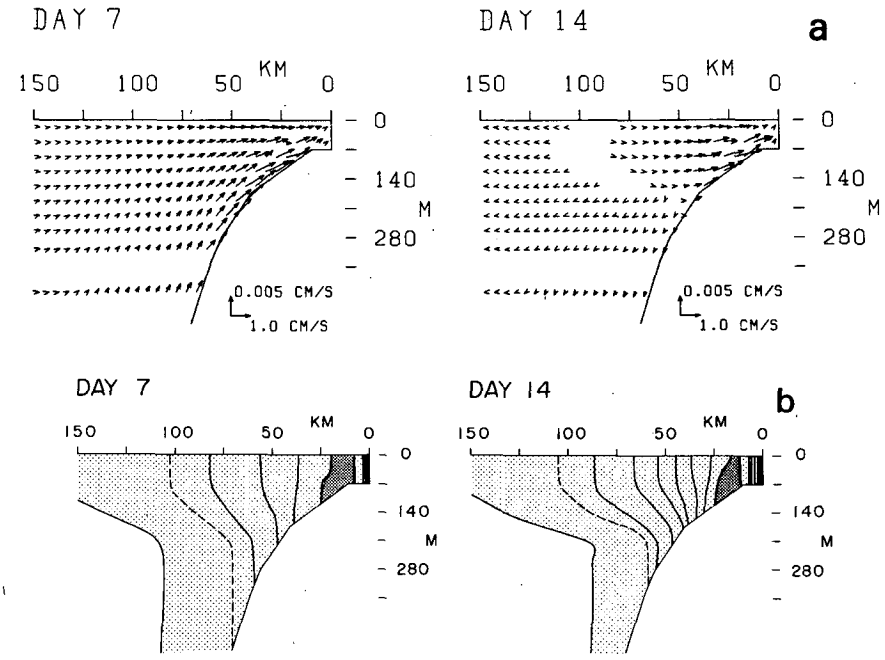

FIG. 7. Onshore–offshore circulation (a) and alongshore flow (b) along the section 150 km north of the forcing region. The contour interval is 4 cm s^{-1} and the shaded areas are for the equatorward flow.

upwelling in the coastal area, can be accounted for by the wave dynamics discussed in Figs. 8 and 9.

In each of the two cases, the momentum and vorticity balances are almost linear. For the equation of density, the dominant balance is $\partial\rho/\partial t + w(\partial\rho(z)/\partial z) \approx 0$, where $\rho(z)$ is the initial density stratification, except where fronts are formed. Thus, the results can be described by linear wave dynamics.

4. Discussion and conclusion

The onshore–offshore circulation, equatorward coastal jet and poleward undercurrent associated with coastal upwelling have been studied with numerical models. The model ocean has a continental shelf–slope uniform in the longshore direction and is forced by the wind stress with a limited longshore extent. The thermocline intersects the shelf–slope, and the internal radius of deformation is smaller than the width of the shelf–slope. This may be a typical situation for the coastal upwelling regions such as those off Oregon and northwest Africa. Two case studies for the different initial (basic) density stratification have been discussed: a thin thermocline for the first case and a thick thermocline for the second.

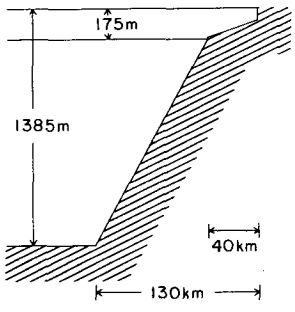

FIG. 8. Schematic view of the idealized two-layer model.

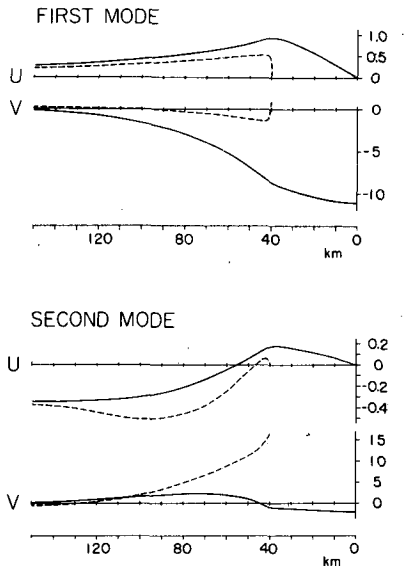

FIG. 9. The offshore and alongshore components of flow as eigenfunctions for the first (top) and the second (bottom) modes against the distance from the coast for long nondispersive waves. The solid lines are for the upper layer and the dashed lines for the lower layer.

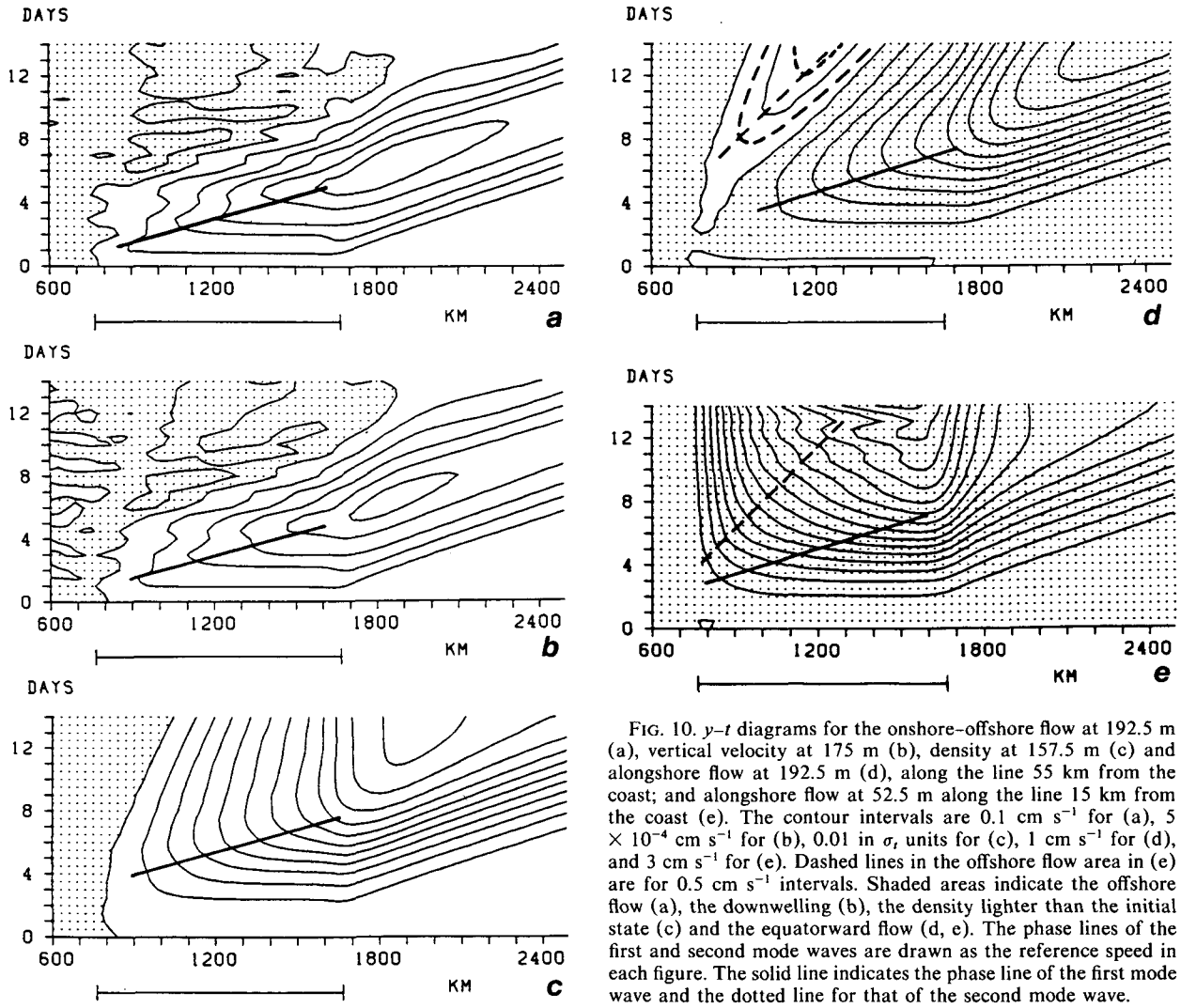

FIG. 10. y–t diagrams for the onshore–offshore flow at 192.5 m (a), vertical velocity at 175 m (b), density at 157.5 m (c) and alongshore flow at 192.5 m (d), along the line 55 km from the coast; and alongshore flow at 52.5 m along the line 15 km from the coast (e). The contour intervals are 0.1 cm s^{-1} for (a), 5 $\times$ 10^{-4} cm s^{-1} for (b), 0.01 in σ_t units for (c), 1 cm s^{-1} for (d), and 3 cm s^{-1} for (e). Dashed lines in the offshore flow area in (e) are for 0.5 cm s^{-1} intervals. Shaded areas indicate the offshore flow (a), the downwelling (b), the density lighter than the initial state (c) and the equatorward flow (d, e). The phase lines of the first and second mode waves are drawn as the reference speed in each figure. The solid line indicates the phase line of the first mode wave and the dotted line for that of the second mode wave.

As the initial response to the onset of the winds, the Ekman offshore flow and the compensating onshore flow are induced and the equatorward flow develops over the shelf-slope. Inside of the forcing region, they have insignificant longshore variations, and the upwelling circulation is balanced in a zonal (offshore, vertical) plane. Then, coastal trapped waves (which are identified neither as internal Kelvin nor as barotropic shelf waves) generated at the southern edge of the forcing region play roles in determining upwelling circulation. When the first mode coastal-trapped wave from the southern edge of the forcing region arrives, the onshore compensating flow offshore of the coastal area begins to decrease in strength, and eventually offshore flow accompanied by downwelling dominates. Thus, the upwelling tends to be confined to the coastal area. For the alongshore flow, the equatorward flow tends to be confined to the coastal area, i.e., the equatorward coastal jet is formed, and the poleward undercurrent develops below the thermocline over the slope. When the second mode wave arrives, the upwelling region tends to be further confined to the coastal area, and

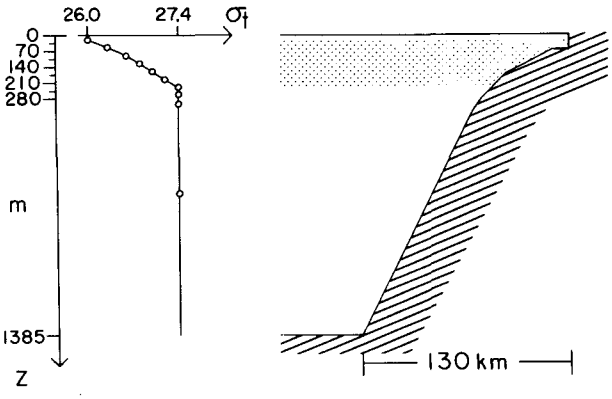

FIG. 11. The initial stratification for case B.

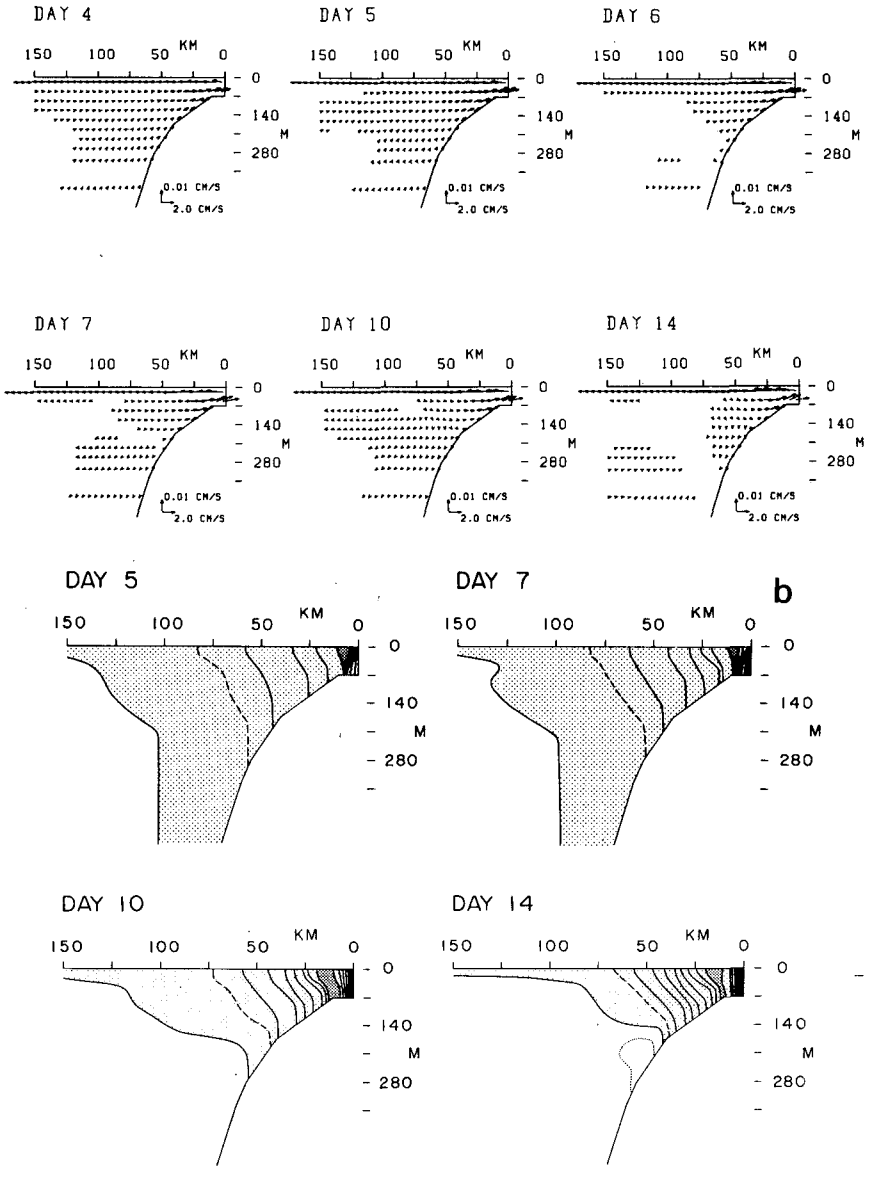

FIG. 12. Sequential patterns of the onshore–offshore circulation (a) and alongshore flow (b) for case B, as in Fig. 4.

the equatorward coastal jet and poleward undercurrent cease to develop. After the first mode wave arrives, the upwelling circulation is balanced three-dimensionally, and the compensation for the upwelling confined to the coastal area is performed by the divergence due to the equatorward coastal jet as well as the onshore flow. The change in basic stratification, i.e., a thicker or thinner thermocline, does not give rise to a significant change in upwelling circulation, i.e., the patterns and evolution of the coastal jet, undercurrent and onshore–offshore circulation are quite similar in both cases. Therefore, it may be concluded that for description of the gross features of the upwelling circulation observed off Oregon and northwest Africa, the lowest two coastal-trapped wave modes, especially the first mode are essential. Of course, the details of the upwelling circulation, especially those in the coastal area, depend on the detailed properties of many coastal-trapped wave modes whose responses yield the forced upwelling circulation.

An additional experiment was carried out for a case where the Coriolis parameter was half that for case A (~70 km for the deformation radius). By this experiment the effects of change in the ratio of the internal radius of deformation to the width of the shelf–slope on the upwelling circulation may be speculated. The evolution of the upwelling circulation can

be accounted for by the coastal-trapped wave dynamics in the same way as before. The onshore–offshore scales of the upwelling circulation become larger. The decrease in propagation speeds of both the first and second mode waves results in a significant intensification of the equatorward coastal jet in spite of the widening of this jet, and in the delay of formation of the poleward undercurrent. Also, an increase in the Ekman transport (τ^y/f) leads to significant intensification of the upwelling in the coastal area in the later stage after the first mode wave from the southern edge arrives.

A case where the distribution of the winds was sinusoidal in the limited longshore extent, like that of Suginohara (1974), was also studied. Although longshore variations of the upwelling circulation caused by the sinusoidal wind distribution were observed in the early stage, the essential results are similar to those discussed before, i.e., associated with the arrivals of the wave modes from the southern edge of the forcing region, changes in the upwelling circulation take place.

In the present study, only short-term upwelling events (two-week events), starting the ocean from rest have been studied. For description of the circulation associated with a short-term upwelling, the lowest two coastal-trapped wave modes, especially the first mode are essential. In the typical coastal upwelling regions, e.g., off Oregon, the upwelling-favorable winds continue to blow throughout the upwelling season with fluctuations both in speed and direction. As the upwelling season starts, the main thermocline starts to rise and forms inclined isopycnals involving fronts formed by the seasonal thermocline. Associated with this thermal structure, there exists a mean alongshore flow over the shelf–slope. The present study may describe the deviations from this mean flow. The effect of the mean field is

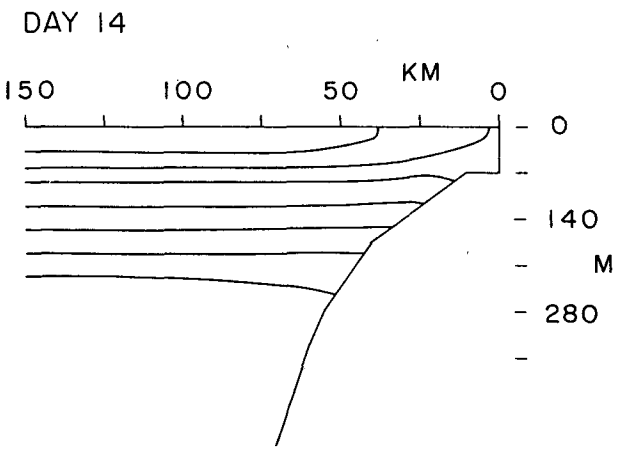

FIG. 13. Density section at the center of the forcing region. The contour interval is 0.2 in σ_t units.

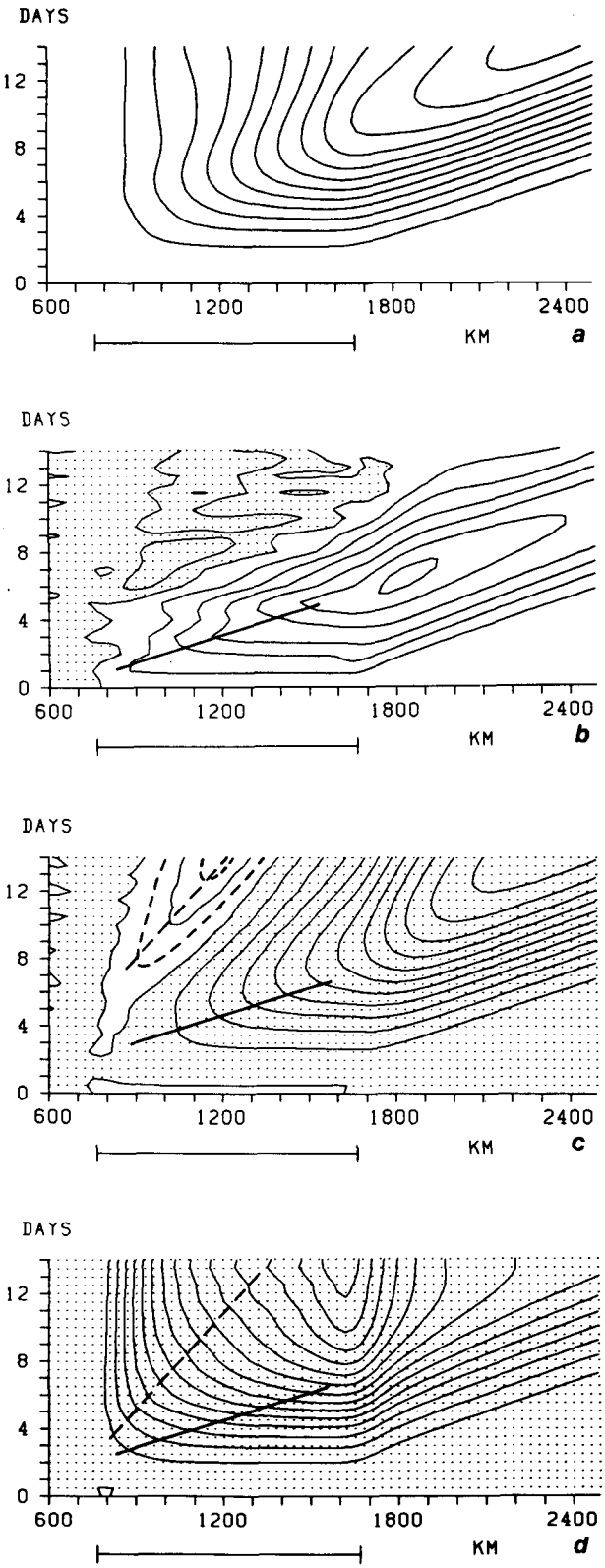

FIG. 14. y–t diagrams for case B. (a) As in Fig. 6 except for the doubled contour interval. (b) As in Fig. 10a. (c) As in Fig. 10d. (d) As in Fig. 10e.

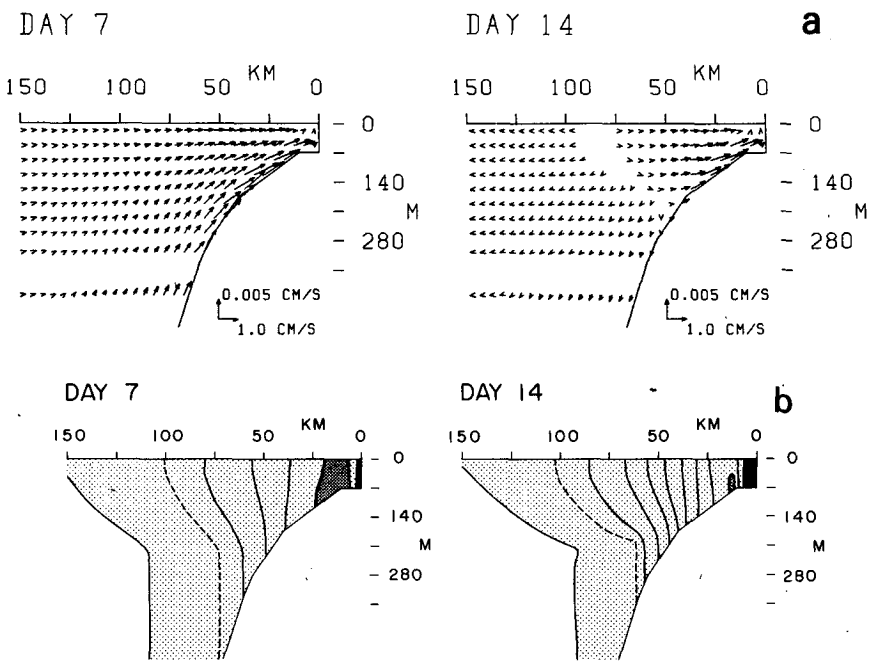

FIG. 15. Onshore-offshore circulation (a) and longshore flow (b) for case B in the same manner as in Fig. 7.

still open for study. For this, a long-time calculation corresponding to the whole upwelling season will be needed, especially for simulating the observations. Effects of heating as well as the β effect should be taken into account in order to accomplish such a long-term calculation. At the same time, the mixing processes need to be adequately parameterized, since the higher wave modes become important for a long-term upwelling as pointed out by McCreary (1981) and Yoon and Philander (1982).

Drastic changes in upwelling circulation caused by changes in winds are frequently observed. The poleward undercurrent and offshore flow in the lower part of the thermocline over the slope seem to be observed during the weak-wind period (Huyer, 1976). Preliminary studies of the effects of changes in winds show that a decrease (increase) in wind speed leads to a significant, apparent increase (decrease) in propagation speed of coastal-trapped waves from the southern edge of the forcing region. The observed evolution of the upwelling circulation associated with a change in winds may be accounted for by the present wave dynamics. The response to a change in the winds will be discussed in the near future.

Acknowledgments. I thank Drs. J. H. Yoon and M. Kawabe for pleasant discussions. Thanks are extended to Drs. K. Kajiura, C. N. K. Mooers and J. P. McCreary for reading the manuscript and making helpful comments. I thank also Ms. T. Osada for drafting the figures and typing the manuscript.

REFERENCES

Allen, J. S., 1980: Models of wind-driven currents on the continental shelf. *Annual Review of Fluid Mechanics*, Vol. 12, Annual Reviews, Inc., 389–433.

Barton, E. D., A. Huyer and R. L. Smith, 1977: Temporal variation observed in the hydrographic regime near Cabo Corveire in the northwest Africa upwelling region, February to April 1974. *Deep-Sea Res.*, **24,** 7–23.

Huthnance, J. M., 1978: On coastal trapped waves: analysis and numerical calculation by inverse iteration. *J. Phys. Oceanogr.*, **8,** 74–92.

Huyer, A., 1976: A comparison of upwelling events in two locations: Oregon and northwest Africa. *J. Mar. Res.*, **34,** 531–546.

——, R. D. Pillsbury and R. L. Smith, 1975: Seasonal variation of the alongshore velocity field over the continental shelf off Oregon. *Limnol. Oceanogr.*, **20,** 90–95.

Kawabe, M., 1982: Coastal trapped waves in a two-layer ocean: Wave properties for a case where the interface intersects a sloping bottom. Submitted to *J. Oceanogr. Soc. Japan.*

McCreary, J. P., 1981: A linear stratified ocean model of the Coastal Undercurrent. *Phil. Trans. Roy. Soc. London*, **A302,** 385–415.

Suginohara, N., 1974: Onset of coastal upwelling in a two-layer ocean by wind stress with longshore variation. *J. Oceanogr. Soc. Japan*, **30,** 23–33.

——, 1977: Upwelling front and two-cell circulation. *J. Oceanogr. Soc. Japan*, **33,** 115–130.

——, 1981: Propagation of coastal-trapped waves at low latitudes in a stratified ocean with continental shelf slope. *J. Phys. Oceanogr.*, **11,** 1113–1122.

Wang, D. P., and C. N. K. Mooers, 1976: Coastal trapped waves in a continuously stratified ocean. *J. Phys. Oceanogr.*, **6,** 853–863.

Yoon, J. H., and S. G. H. Philander, 1982: Formation of the coastal undercurrent. Submitted to *J. Oceanogr. Soc. Japan.*

Yoshida, K., 1980: The coastal undercurrent—a role of longshore scales in coastal upwelling dynamics. *Progr. Oceanogr.*, **9,** 83–131.